arXiv:0812.4493v2 [astro-ph] 4 May 2009

Probing Dark Energy at Galactic and Cluster Scales

David F. Mota

D.Mota@thphys.uni-heidelberg.de

Institute for Theoretical Physics, University of Heidelberg, 69120 Heidelberg,Germany

Lab. de Physique Theorique et Astroparticules, CNRS Universite Montpellier II, France

Abstract. We investigate dark matter halo properties as a function of a time–varying dark energy equation of state. The dynamics of the collapse of the halo is governed by the form of the quintessence potential, the time evolution of its equation of state, the initial conditions of the field and its homogeneity nature in the highly non–linear regime. These have a direct impact on the turnaround, virialisation and collapse times, altering in consequence the non–linear density contrast and virial radius. We compute halo concentrations using the Eke, Navarro & Steinmetz algorithm, examining two extreme scenarios: first, we assume that the quintessence field does not exhibit fluctuations on cluster scales and below - homogeneous fluid; second, we assume that the field inside the overdensity collapses along with the dark matter - inhomogeneous fluid. The Eke, Navarro & Steinmetz prescription reveals, in general, higher halo concentrations in inhomogeneous dark energy models than in their homogeneous equivalents. Halo concentrations appear to be controlled by both changes in formation epochs of the halo cores as well as by differing virialisation overdensities. We derive physical halo properties in all models and discuss their observational implications. We examine two possible methods for comparing observations with theoretical predictions. The first method works on galaxy cluster scales and consists of fitting the observed X–ray cluster gas density distributions to those predicted for an NFW profile. The second method works on galaxy scales and involves the observational measurement of the so–called central density parameter.

1. Introduction

Observations of the Cosmic Microwave Background temperature anisotropy reveal that a mysterious constituent with negative pressure, so–called dark energy, accounts for 70 percent of today's mass–energy budget and is causing the expansion of the universe to accelerate [1]. These observations are in remarkable concord with the observations of distant supernovae [2].

The present–day challenge in cosmology is to discover the physical nature of dark energy. Candidates for this unknown entity include the cosmological constant, a dynamic cosmic field, commonly designated quintessence, which varies across space and changes with time, and a possible modification of General Relativity at large scales [3–5].

Although the physical nature of dark energy is undisclosed, one can explore its effects on cosmic structure formation, in particular one can study its implications for the number density of dark matter halos and their density profiles. In this respect, significant progress has been made by several authors who performed numerical N–body simulations in dark energy models [6–10]. These investigations are imperative for cosmological studies that rely on these ingredients to measure dark energy. Examples of this studies include semi-analytical studies of strong lensing statistics [11–13] and weak lensing number counts [11, 14].

In this paper, we investigate how halo properties change in cosmological models with dynamical dark energy. This work extends upon previous studies in that we examine halo properties as a function of a time–varying dark energy equation of state, covering four types of potentials, and its homogeneity nature in the highly non–linear regime. We utilise the predictions of the spherical collapse model, such as the virial overdensity, obtained by [15, 16], and calculate halo concentrations using the semi-analytical algorithm of Eke, Navarro & Steinmetz (ENS) [17]. We then derive physical halo properties in all models and discuss their observational implications.

The behaviour of linear perturbations in a scalar field and its effect on structure formation has been investigated by a number of authors. However, the behaviour of quintessence during the non–linear gravitational collapse is not well understood and is currently under investigation (see e.g. [15, 16, 23–25] for recent work). Usually, it is assumed that the quintessence field does not exhibit density fluctuations on cluster scales and below. The reason for this assumption is that, according to linear perturbation theory, the mass of the field is very small (the associated wavelength of the particle is of the order of the Hubble radius) and, hence, it does not feel matter overdensities of the size of tenth of a Mpc or smaller [26].

The assumption of neglecting the effects of matter perturbations on the evolution of dark energy at small scales is indeed a good approximation when perturbations in the metric are very small. However, care must be taken when extrapolating the small–scale linear–regime results to the highly non–linear regime. Then, locally the flat FRW metric is no longer a good approximation to describe the geometry of overdense regions.

Highly non–linear matter perturbations could, in principle, modify the evolution of perturbations in dark energy considerably, and these could, in turn, backreact and affect the evolution of matter overdensities. Moreover, it is natural to think that once a dark matter overdensity decouples from the background expansion and collapses, the field inside the cluster feels the gravitational potential inside the overdensity and its evolution will be different from the background evolution. This is a general feature of many cosmological scalar fields whose properties depend on the local density of the region they "live in" [43].

[35] suggested that the quintessence field could have an important impact in the highly non—linear regime. [24, 31] noted that the quintessence field could indeed be important on galactic scales. It was put forward by [30] that it could in fact be responsible for the observed flat rotation curves in galaxies. Other authors [37] discussed more exotic models, based on tachyon fields, and argued that the equation of state is scale–dependent.

If it turns out that the effects of dark matter density perturbations and metric influence perturbations of quintessence on small scales, this could significantly change our understanding of structure formation on galactic and cluster scales. [15, 16, 39] have shown that properties of halos, such as the density contrast and the virial radius, depend critically on the form of the potential, the initial conditions of the field, the time evolution of its equation of state and on the behaviour of quintessence in highly non–linear regions. In reality, the dependence on the inhomogeneity of dark energy is only important for some dark energy candidates. If the dark energy equation of state is constant, the differences between the homogeneous and inhomogeneous cases are small, as long as the equation of state w does not differ largely from $w = -1$ [15, 16]. Thus, for constant equation of state, the fitting formulae for the cold dark matter (CDM) density contrast presented in the literature [26, 27], do not change drastically, even if inhomogeneities in the dark energy component are taken into account.

The paper is organised as follows. In section 2 we describe briefly the spherical collapse model and its dependence on the homogeneity nature of dark energy. In section 3 we calculate halo concentrations in both homogeneous and inhomogeneous dark energy models. We diagnose observational methods to measure physical halo properties in section 4. Section 5 discusses the results and draws the conclusions.

2. The spherical collapse model and the homogeneity nature of dark energy

We consider a flat, homogeneous and isotropic background universe with scale factor $a(t)$. Since we are interested in the matter dominated epoch, when structure formation starts, we fill the universe with cold dark matter of density $\rho_{\rm m} \propto a^{-3}$ and a dark energy fluid with energy density ρ_ϕ. The equations that describe the background universe are (we set $\hbar = c \equiv 1$ throughout the paper):

$$3H^2 = 8\pi G\left(\rho_{\rm m} + \rho_\phi\right) \tag{1}$$

$$\dot{\rho}_\phi \;\; = \;\; -\,3H(1+w_\phi)\rho_\phi \tag{2}$$

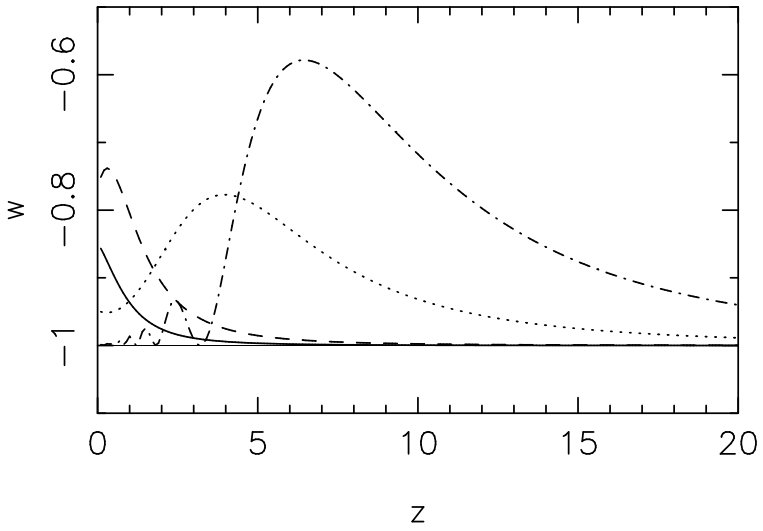

Figure 1. Dark energy equation of state in the background universe as a function of redshift, z. Thick solid line - [33], dashed line - [45], dashed–dotted line - [29], dotted line - [36], thin solid line - cosmological constant.

where $H \equiv \dot{a}/a$ is the Hubble rate. When $w_\phi = -1$ dark energy is the vacuum energy density. If dark energy is a scalar field ϕ (quintessence), $\rho_\phi = \frac{1}{2}\dot{\phi}^2 + V(\phi)$ and $P_\phi = \frac{1}{2}\dot{\phi}^2 - V(\phi)$, where $V(\phi)$ is the scalar field potential. In this case, it is useful to rewrite equation (2) as

$$\ddot{\phi} + 3H\dot{\phi} + V^{'} = 0 \tag{3}$$

where the prime represents a derivative with respect to ϕ.

In this paper, we consider four examples of quintessential potentials:

- The double exponential potential [33]:

$$V(\phi) = M\left(\exp(\beta\phi) + \exp(\gamma\phi)\right). \tag{4}$$

- The exponential potential with inverse power [45]:

$$V(\phi) = M\left(\exp(\gamma/\phi) - 1\right) \tag{5}$$

- The Albrecht–Skordis potential [29]:

$$V(\phi) = M\left(A + (\phi - B)^2\right)\exp(-\gamma\phi) \tag{6}$$

- The supergravity–motivated potential [36]:

$$V(\phi) = M\exp(\phi^2)/\phi^\gamma \tag{7}$$

We choose the parameters in the potentials and the initial conditions in the background such that we obtain the following present–day cosmological parameters: $\Omega_m = 0.3$, $\Omega_\phi = 0.7$,$H_0 = 100\,\mathrm{h\,km\,s^{-1}\,Mpc^{-1}}$ with $h = 0.7$, and $-1 \leq w_\phi \leq -0.8$. The background time evolution of the equation of state for each model is shown in figure 1.

The evolution of a spherical overdense patch of scale radius $R(t)$ is given by the Raychaudhuri equation:

$$3\ddot{R} = -4\pi GR\left(\rho_{\mathrm{m_c}} + \rho_{\phi_c}(1 + 3w_{\phi_c})\right) \tag{8}$$

Note that it would be wrong to use the Friedmann equation for a closed universe with a constant curvature k, since the former can vary in time [26, 27]. In the halo, the evolution of ρ_{ϕ_c} and $\rho_{\mathrm{m_c}}$ is given by

$$\dot{\rho}_{\phi_c} = -3\frac{\dot{R}}{R}(1 + w_{\phi_c})\rho_{\phi_c} + \Gamma \tag{9}$$

and $\rho_{\mathrm{m_c}} \propto R^{-3}$ due to mass conservation. Once again, in the case of a scalar field, equation (9) can be written as [15, 16]

$$\ddot{\phi}_c + 3\frac{\dot{R}}{R}\dot{\phi}_c + V_c'(\phi_c) = \frac{\Gamma}{\dot{\phi}_c} \tag{10}$$

where ϕ_c is the field inside the overdensity (the lowerscript distinguishes it from the background value) and $V_c = V(\phi_c)$ is its potential. The quantity Γ describes the energy loss of dark energy inside the dark matter overdensity, as this component does not necessarily follow the collapse of dark matter, and energy can formally flow out of the system. As such, Γ encodes in how far dark matter non–linearities act on the dark energy component.

We will make two assumptions for Γ. In the first case, the quintessence field is assumed to be smooth throughout space. This corresponds to

$$\Gamma = -3\left(\frac{\dot{a}}{a} - \frac{\dot{R}}{R}\right)\dot{\phi}_c^2, \tag{11}$$

$\phi_c(t_i) = \phi(t_i)$ and $\dot{\phi}_c(t_i) = \dot{\phi}(t_i)$, which implies $\phi_c(t) = \phi(t)$ at all times, and is the standard assumption made in the literature. In the second case, we assume that the field follows the dark matter collapse from the very beginning. That is, we assume $\Gamma = 0$.

Clearly, the values of Γ chosen are not realistic, but they mark off two extreme scenarios. At very late times, during the collapse of the dark matter, especially when the density contrast in dark matter is very large ($\delta_{\mathrm{m}} \gg 1$), the field should no longer feel the background metric, i.e. it decouples from the background expansion. In this regime, the evolution of dark energy could be different and influence the details of the collapse. Only when Γ is quantified and the boundary conditions between the outer and inner metrics are properly understood, will the spherical collapse model be able make to solid predictions. An estimate of Γ can only be obtained from a general relativistic treatment. This could be achieved in two ways. One way would be to develop a swiss cheese model. Another way would be to perform N–body simulations that take into account the effects of dark energy perturbations in smaller scales. This is however out of the scope of this article.

Throughout the paper, we refer to a homogeneous dark energy model as a model where dark energy does not exhibit fluctuations on cluster scales and below (Γ given by equation 11). This designation may be seen as somewhat abusive in the sense that these models are inhomogeneous on scales larger than cluster scales. In truth, only the cosmological constant model is homogeneous across all

space. We refer to a inhomogeneous dark energy model as a model where dark energy does exhibit fluctuations on cluster scales and below ($\Gamma = 0$). The terms homogeneous/inhomogeneous are therefore associated with cluster scales and below, here taken as the scales of interest.

We evolve the spherical overdensity from high redshift until its virialisation occurs (see [15, 16] for details). Figure 2 plots the CDM density contrast, $\Delta_{\rm vir} \equiv \frac{\rho_{\rm m_c}}{\rho_{\rm crit}}$, as a function of redshift. It is clear from the figure that an homogeneous dark energy fluid is very similar to a cosmological constant. Major differences occur in the inhomogeneous case. These are discussed in the following section.

3. Halo properties

The dark matter halo is modelled with the NFW profile [44]:

$$\rho(r) = \frac{\rho_s}{(r/r_s)(1+r/r_s)^2} \tag{12}$$

where r_s is the characteristic length and ρ_s is the characteristic density scale, $\rho_s = \delta_c \rho_{\rm crit}$, where $\rho_{\rm crit} = 3H^2/8\pi G$ is the critical density for closure and

$$\delta_c = \frac{\Delta_{\rm vir}}{3} \frac{c_{\rm vir}^3}{ln(1+c_{\rm vir}) - c_{\rm vir}/(1+c_{\rm vir})} \tag{13}$$

is the characteristic density contrast. The halo concentration is defined as $c_{\rm vir} \equiv r_{\rm vir}/r_s$ where $r_{\rm vir}$ is the radius of a sphere containing a mean density $\Delta_{\rm vir}$ times the critical density:

$$M_{\rm vir} = \frac{4\pi}{3} r_{\rm vir}^3 \Delta_{\rm vir} \rho_{\rm crit}. \tag{14}$$

At small radii ($r \ll r_s$) $\rho(r) \sim r^{-1}$, and at large radii ($r \gg r_s$) $\rho(r) \sim r^{-3}$. The NFW profile appears to be a good fit to numerically simulated halos over a wide range of masses in various cosmological scenarios. Although the exact inner slope is under debate, there is general consensus that the density profile steepens at large radii.

3.1. Halo concentrations

Numerical simulations repeatedly show that the later a halo forms the less concentrated it is. This appears as a reflection of the smaller cosmic density at later cosmic epochs. In hierarchical structure formation models less massive halos form earlier than more massive ones, hence the former are more concentrated than the latter.

We use the prescription of [17] to calculate dark matter halo concentrations. This prescription consists of a simple analytic algorithm that was found to reproduce well the mass and redshift dependence of concentrations obtained from high–resolution N–body simulations performed in various cosmological models, in particular in a flat model with a cosmological constant.

One should, however, point out that the ENS model is by no means the only viable prescription. In fact, it is just one of a number of theoretical models for how

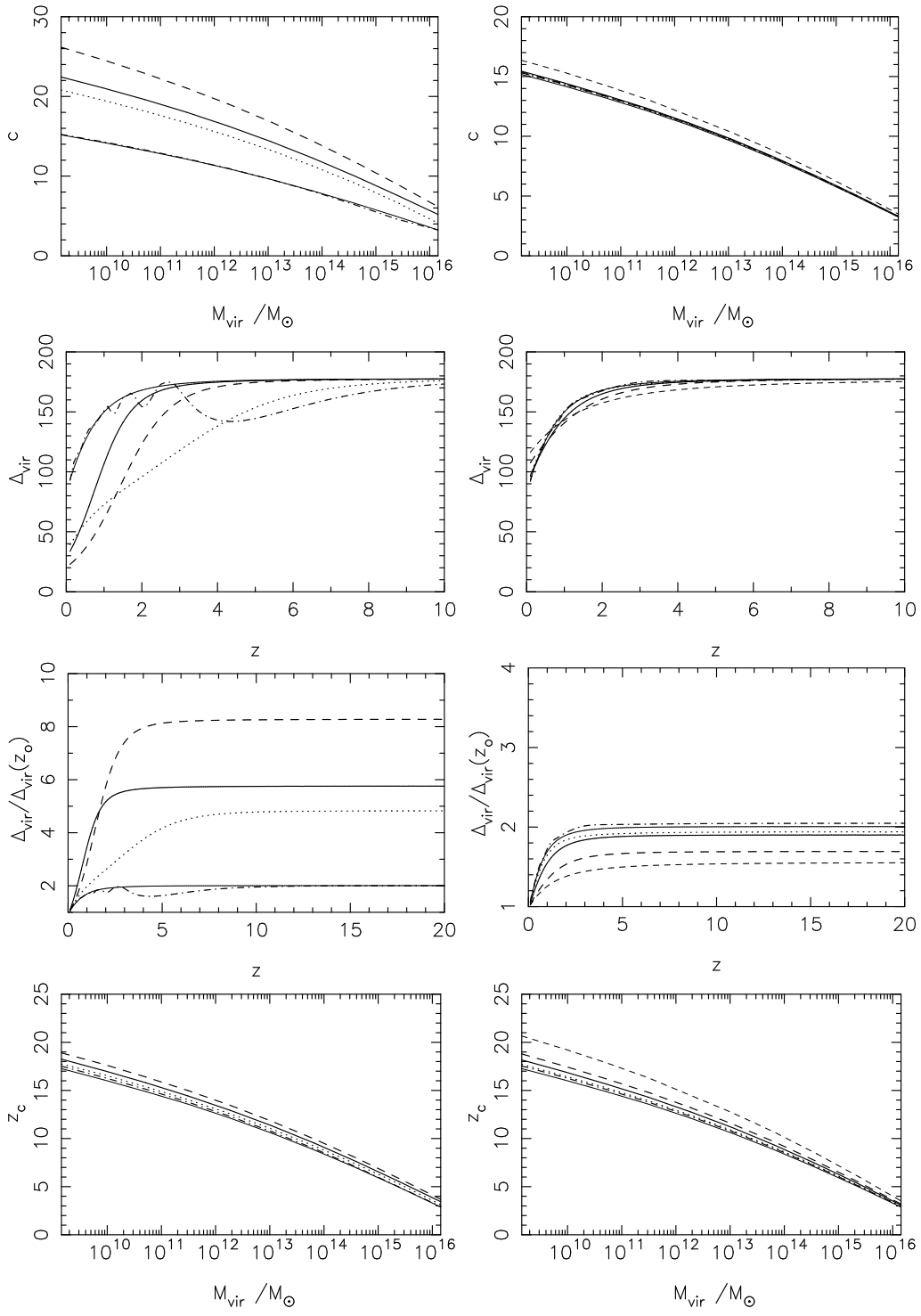

Figure 2. *left* four inhomogeneous dark energy models (thick solid line - [45], dashed line - [36], dot–dashed line - [29], dotted line - [33] plus a cosmological constant model (thin solid line); *right* six homogeneous dark energy models (thick solid line - [45], thick dashed line - [36], dot–dashed line - [29], dotted line - [33], thin dashed line - constant equation of state $w = -0.6$, thin solid line - cosmological constant); *upper panel* dark matter halo concentrations; *upper middle panel* non–linear overdensity at virialisation; *lower middle panel* non–linear overdensity at virialisation normalised at z_o; *lower panel* characteristic formation redshift as defined by [17].

the concentration mass relation arises. Examples of other models are the original NFW model, the Bullock et al. model [18], or the recent extension of this by Maccio et al. [19]. Some of these studies produced results in agreement with ENS (e.g. [21]), others find a mass and redshift dependence that contradicts the ENS model (e.g. [20], [22]). At present the matter has not been settled, and it is not possible to identify one model that works better than all of the others. In this work we will restric ourselves to the ENS model. A Further investigation using and comparing other prescriptions will appear in a near future work [50].

The ENS algorithm relates halo properties with the physics of halo formation as follows:

$$c_{\rm vir}^3 = \frac{\Delta_{\rm vir}(z_c)}{\Delta_{\rm vir}(z_o)} \frac{\Omega_{\rm m}(z_o)}{\Omega_{\rm m}(z_c)} \left(\frac{1+z_c}{1+z_o}\right)^3 \tag{15}$$

which results from setting the core density to the spherical top–hat density at the characteristic formation epoch. z_o is the redshift at which the halo is identified which, is assumed to be the redshift at which the halo as a whole collapses and virialises. The characteristic formation epoch (also designated rapid–collapse epoch), z_c, is associated with the collapse time of the halo subunits. This occurs at the time when the rapid mass accretion rate drops below a fixed value. Thereafter, the halo evolves and its virial radius and halo mass grow through minor mergers and diffuse mass accretion, while the characteristic length r_s remains essentially equal [8, 47]. This process continues until the halo as a whole finally collapses and virialises. The rapid–collapse epoch of a halo of mass M depends on the linear growth factor, $D(z)$, the amplitude and shape of the matter power spectrum, and on a single free parameter C_σ whose value can be found which yields concentration values that match the results from N–body simulations. More explicitly, [17] define the collapse redshift as:

$$D(z_c)\sigma_{\rm eff}(M_s) = \frac{1}{C_\sigma} \tag{16}$$

where $D(z)$ is the linear growth factor and $\sigma_{\rm eff}$ is an effective amplitude of the power spectrum that [17] utilise to modulate $\sigma(M)$ in order to model WDM models. This effective amplitude is computed at M_s, the mass enclosed within the radius at which the NFW circular velocity reaches its maximum, $r_{\rm max} = 2.17 r_s$.

[17] found that $C_\sigma = 28$ gives good agreement with the N–body simulations effectuated in a flat cosmological constant model. [7] have recently performed high–resolution numerical simulations in dark energy models with constant and time–varying equation of state (including Ratra–Peebles and SUGRA models) and have shown that the mass dependence and redshift evolution of concentrations is in conformity with the [17] prescription with $C_\sigma = 28$. Moreover, these authors have demonstrated for the first time with numerical simulations that concentrations are indeed larger in dark energy models as a consequence of halos forming earlier in these models when compared to the cosmological constant model. This confirms the predictions of [34] and [12] which were based on the analytic algorithm of [17]

In this work we assume that the [17] prescription remains valid for models with inhomogeneous dark energy, once all the cosmological functions inherent to the algorithm are specified accordingly. This may in fact be a strong assumption. In particular, the value assumed for the fitting parameter $C_\sigma = 28$ might not be the correct one. However, this is the only reference value one has at present. Up until now, there are no numerical simulations which investigate the effects of dark energy on the internal dynamics of the halo formation. Dark energy has only been incorporated in the background evolution. Both its pressure and energy density have not even been considered to contribute to the local gravitational potential inside overdensities. Although in a very simplified way, the first studies which took into consideration such contributions were the N–body simulations performed by [41] in the case of coupled quintessence.

For the shape of the linear matter power spectrum we adopt the fitting formula of [40] for QCDM models and the [32] fitting formula for the ΛCDM model using the modification of [46] in order to account for the baryons. We fix the primordial power spectrum index to $n = 1$ and the baryon density to $\Omega_b h^2 = 0.02$. The normalisation of the power spectrum is set by σ_8, the *rms* linear density fluctuation in spheres of $8\,\mathrm{h}^{-1}\,\mathrm{Mpc}$, which we choose to be $\sigma_8 = 0.9$.

3.1.1. Inhomogeneous versus homogeneous models Figure 2 shows halo concentrations for all the models studied in this paper (on the left - inhomogeneous dark energy models plus a cosmological constant model for comparison, on the right - homogeneous dark energy models, including also the cosmological constant model for comparison). Also shown are the rapid–collapse redshifts, z_c (as defined by [17]) and the non–linear overdensity at virialisation, Δ_{vir}, for the respective models.

The upper panel indicates that the [17] prescription predicts, in general, larger halo concentrations in inhomogeneous dark energy models than in homogeneous ones. This is however model dependent. For instance, the [36] inhomogeneous model is the model with the highest concentrations which are nearly a factor of two higher than the cosmological constant model or its homogeneous counterpart. In contrast, the inhomogeneous [29] model is almost indistinguishable from the cosmological constant model and its homogeneous counterpart. The inhomogeneous [33] model and [45] model lie in between the cosmological constant model and the [36] inhomogeneous model. The former reveal concentrations higher than their homogeneous counterparts. Furthermore, all homogeneous models present concentrations of the same order of the cosmological constant model.

This is interpreted as a combined effect arising from the ratios that enter as factors in formula (15). The matter density ratio is essentially equal in all the models. Although there is some difference on the rapid–collapse redshifts (lower panel), the overall change in concentrations for inhomogeneous models is primarily owing to the contrast in non–linear overdensity at virialisation (middle panels). The latter depends on the clustering properties of the quintessence field. While at high virialisation redshifts, all models

predict $\Delta_{\rm vir} \approx 178$, significant deviations may occur at low virialisation redshifts due to the fact that dark energy starts to dominate in the background universe. Indeed, for inhomogeneous dark energy ($\Gamma = 0$), $\Delta_{\rm vir}$ can differ by a factor of four or more at low virialisation redshifts. This is nevertheless model dependent. In the [29] model, the field behaves like a cosmological constant in the background (see Fig 1). Hence, one would expect small differences between that and the ΛCDM model. This is indeed the case, because $\dot{\phi}_{\rm c} \approx 0$ which, in turn, implies $\Gamma \approx 0$, as it can be seen from equation (11). Thus, in this model, the fluctuations in the quintessence field remain small and the field is almost homogeneous. In fact, the non–linear overdensity for the Albrecht & Skordis model oscillates around the cosmological constant model which explains the virtually coinciding concentrations in these two models. One should point out that what really characterises the differing ratios $\Delta_{\rm vir}/\Delta_{\rm vir}(z_o)$, and consequent varying concentrations in the various models, is the value of the non–linear overdensity at z_o (here, $z_o = 0.05$) since at high redshifts, where the rapid–collapse of the halo happens, its value is practically equal in all models ‡.

In effect, one can see that $\Delta_{\rm vir}$ at low redshifts can differ by a factor of two between the cosmological constant model and an inhomogeneous model, but differs only about ten per cent between the cosmological constant model and an homogeneous dark energy model. As a result, homogeneous dark energy models exhibit less noticeable differences in concentrations (unless one considers high values of w) and these are mostly inherent to the differing rapid–collapse redshifts which are highest for the model with constant equation of state $w = -0.6$. Indeed, for homogeneous dark energy models concentrations are larger as w increases owing to structures forming earlier. This is in agreement with the previous findings from high–resolution numerical simulations [6–8] which confirm that halos keep a memory in their central regions of the mean density of the universe at the characteristic formation epoch. Why do all the models, both homogeneous and inhomogeneous models, exhibit analogous values of z_c? It is because z_c is calculated from linear theory, depending solely on the matter power spectrum and on the linear growth factor. Hence, this depends on the background cosmology only and not on the non–linear physics dynamics of the halo that distinctively categorises the inhomogeneous dark energy models and from which one can infer the linear overdensity at collapse. The omission of the latter in the [17] prescription may be invalid, and thus needs to be tested.

To summarise, the trends presented in Fig. 2 for halo concentrations in the two classes of models studied appear to be controlled both by differing formation histories as well as by varying virialisation overdensities. While for inhomogeneous models, the virialisation overdensities constitute the dominant factor, for homogeneous models it is the differing formation histories that account for the changes in concentrations.

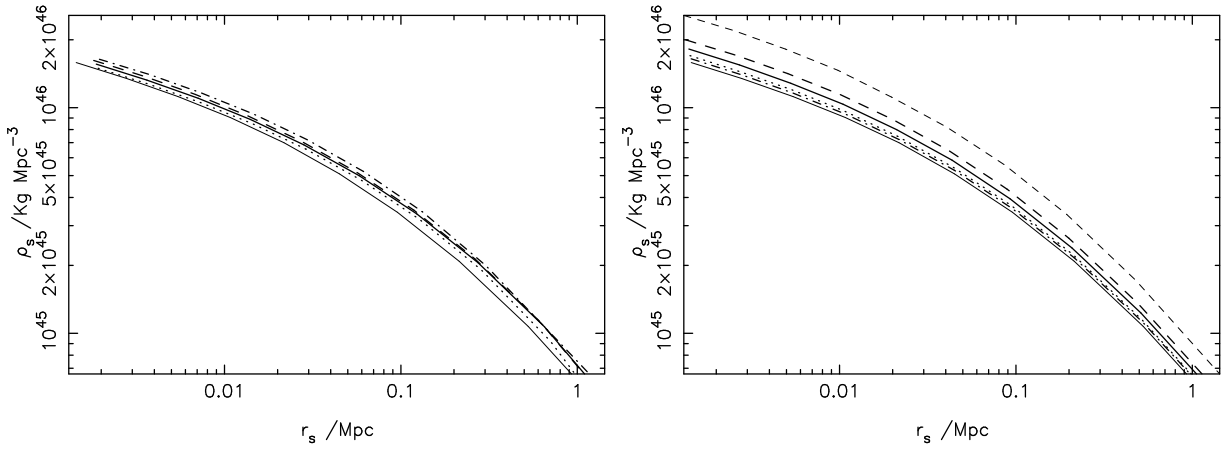

Figure 3. *left* ρ_s vs. r_s relation in four inhomogeneous dark energy models (thick solid line - [45], dashed line - [36], dot–dashed line - [29], dotted line - [33] plus a cosmological constant model (thin solid line); *right* the same relation in six homogeneous dark energy models (thick solid line - [45], thick dashed line - [36], dot–dashed line - [29], dotted line - [33], thin dashed line - constant equation of state $w = -0.6$, thin solid line - cosmological constant).

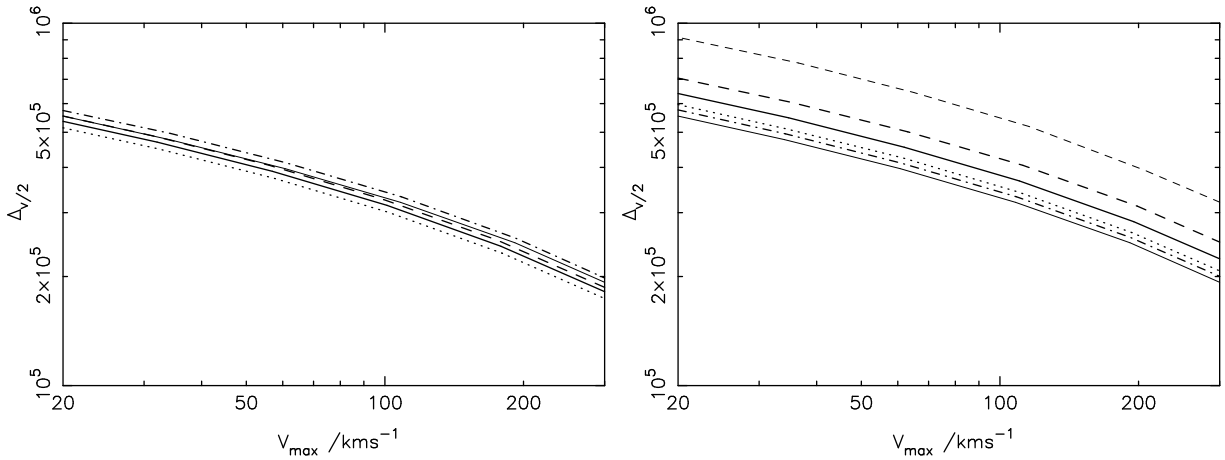

Figure 4. *left* $\Delta_{v/2}$ vs. $V_{\rm max}$ in four inhomogeneous dark energy models (thick solid line - [45], dashed line - [36], dot–dashed line - [29], dotted line - [33] plus a cosmological constant model (thin solid line); *right* the same relation in six homogeneous dark energy models (thick solid line - [45], thick dashed line - [36], dot–dashed line - [29], dotted line - [33], thin dashed line - constant equation of state $w = -0.6$, thin solid line - cosmological constant).

4. Observational Implications

The effect of dark energy on halo properties is expected to be imprinted on observable quantities. Unfortunately, the predicted $c_{\rm vir} - M_{\rm vir}$ relation is not itself directly observable.

Note that [38] have determined the $c_{\rm vir} - M_{\rm vir}$ relation using the dynamical properties of dark halos derived from the distribution of galaxies in massive systems (groups or clusters) and the rotation curves in less massive systems (dwarf, low surface

‡ it approaches the Einstein–de–Sitter model $\Delta_{\rm vir} \approx 178$.

brightness and spiral galaxies) and have found that the observational data are grossly consistent with the theoretical predictions of a flat cosmological constant model on a mass range $10^{10} - 10^{15} M_{\odot}$. However, measurements of halo concentrations through the aforementioned observational method, as well as via weak and/or strong lensing cluster measurements, cannot be used to discriminate cosmological models since observational estimations of their values rely on $\Delta_{\rm vir}$ and $\rho_{\rm crit}$ which are cosmology–dependent but unobservable.

In the following, we examine two possible methods for comparing observations with theoretical predictions. The first method works on galaxy cluster scales and consists of fitting the observed X–ray cluster gas density distributions to those predicted for an NFW profile. [42] have analytically shown that the density distribution of an isothermal gas cloud with temperature T_X, in hydrostatic equilibrium, within an NFW dark matter halo is:

$$\rho_{gas}(r) = \rho_{gas}(0) e^{-\alpha} (1 + r/r_s)^{\alpha/(r/r_s)} \tag{17}$$

where $\alpha = 4\pi G \mu m_p \rho_s r_s^2 / k T_X$ and μ and m_p designate the mean molecular weight and the proton mass, respectively. The best–fit parameters are thus α and r_s, or, alternatively, if one utilises the X–ray temperature, ρ_s and r_s. [48] have applied this technique to an ensemble of 63 X–ray luminous clusters and have determined (assuming a flat cosmological constant model) a best–fit $c_{\rm vir} - M_{\rm vir}$ relation. Here, we look directly at the quantities ρ_s and r_s which are not dependent on cosmology–dependent but unobservable quantities such as $R_{\rm vir}$, although comparison with observations rests on assumptions such as the hydrostatic equilibrium and an isothermal temperature profile of the intracluster gas.

The second method works on galaxy scales and involves the observational measurement of the so–called central density parameter proposed by [28]. This parameter is defined as the mean dark matter overdensity within the radius, $r_{V/2}$, where the galaxy rotation curve is one half of its maximum, $V_{\rm max}$:

$$\Delta_{V/2} = \frac{1}{2} \left(\frac{V_{\rm max}}{H_0 r_{V/2}} \right)^2 . \tag{18}$$

The link between theory and observations can be made through the $\Delta_{V/2} - V_{\rm max}$ relation, where $V_{\rm max}$ works as a measure of the absolute size of the halo. As pointed out by [49], $\Delta_{V/2}$ has the advantage of being defined without reference to any particular density or velocity profile. Theoretically, the maximum velocity of a NFW halo is given by [49]:

$$V_{\rm max}^2 \simeq 0.216 V_{\rm vir}^2 \frac{c_{\rm vir}}{ln(c_{\rm vir}) - c_{\rm vir}/(1 + c_{\rm vir})} \tag{19}$$

where $V_{\rm vir}$ is the virial velocity and $V_{\rm vir}^2 \equiv G M_{\rm vir} / R_{\rm vir}$. In addition, $r_{V/2} \simeq 0.13 r_s$ for a NFW profile. Incorporating equation 19 into equation 18 yields the expected $\Delta_{V/2}$ in theory. This can be computed for any cosmological model given $c_{\rm vir}$ and $\Delta_{\rm vir}$. Comparison with observational data relies, however, on the crucial assumption that baryons have not substantially modified the dark matter profile. This assumption is

weakened, but not unambiguously removed, if observations are focused on low–surface brightness and dwarf galaxies which are believed to be dominated by dark matter.

We now look at the theoretical predictions from both methods. Fig. 3 plots the theoretical relation $\rho_s - r_s$ expected in the various cosmological models for halos at redshift $z_o = 0.05$. Fig. 4 presents the theoretical relation $\Delta_{V/2} - V_{\rm max}$ expected in the same cosmological models for halos at redshift $z_o = 0.05$. Surprisingly, one observes that, contrary to what one might have expected, inhomogeneous models show less pronounced differences in both ρ_s and $\Delta_{V/2}$ than homogeneous models. Moreover, the inhomogeneous lines, in particular, do not reflect the anticipated $c_{\rm vir}$ trends at fixed mass. This occurs because ρ_s and $\Delta_{V/2}$ depend not only on $c_{\rm vir}$ (exactly on $c_{\rm vir}^3/(ln(c_{\rm vir}) - c_{\rm vir}/(1 + c_{\rm vir}))$) but also on $\Delta_{\rm vir}(z_o)$ § which somewhat counteracts with $c_{\rm vir}$. In effect, for inhomogeneous models, the non–linear overdensities at virialisation decrease as the concentrations increase. The homogeneous models, conversely, present differences among themselves that can be about a factor 1.5. In the next section we discuss the feasibility of the aforementioned techniques to actually discriminate cosmological models.

Finally, the ability of a cluster to lens a background object, a galaxy or a quasar, depends critically on the halo profile and consequently on its concentration, therefore the influence of dark energy (and its homogeneity nature) on halo concentrations may be tested, albeit indirectly, through the observational statistics of multiply imaged quasars or giant arcs of galaxies. [12] have shown that the cross–section for quasar multiple imaging is increased for homogeneous dark energy models with $w > -1$, owing to halo concentrations being larger in those models. The expected increase on halo concentrations in models where dark energy is inhomogeneous may also produce an effect on the lensing cross–section. This remains to be investigated.

5. Discussion and Conclusions

We have studied halo properties in models with dynamical dark energy. This work extends upon previous studies in that we investigate halo properties as a function of a time–varying dark energy equation of state, covering four classes of potentials, and its homogeneity nature in the highly non–linear regime.

The dynamics of the collapse of the halo is regulated by the form of the dark energy potential, the time evolution of its equation of state, the initial conditions of the field and its homogeneity properties in the highly non–linear regime. These have a direct influence on the turnaround, virialisation and collapse times, altering in consequence the (non–linear) density contrast and virial radius [15, 16].

As for the homogeneity nature of dark energy in the highly non–linear regime, we have examined two extreme scenarios: first, we assumed that the quintessence field does not exhibit fluctuations on cluster scales and below - homogeneous fluid; second,

§ ρ_s has an additional dependence on $\rho_{\rm crit}$.

we supposed that the field inside the overdensity collapses along with the dark matter - inhomogeneous fluid.

We have computed halo concentrations using the algorithm of [17] and have derived physical halo properties expected within this analytical treatment. We find that the [17] prescription displays, in general (the exception being the [29] model), higher halo concentrations in inhomogeneous dark energy models than in their homogeneous equivalents. The [36] inhomogeneous model is the model with the highest concentrations which are nearly a factor of two higher than the cosmological constant model or its homogeneous counterpart. For homogeneous dark energy models concentrations are larger as w increases owing to structures forming earlier. This is in agreement with previous findings from high–resolution numerical simulations which demonstrate that halos keep a memory in their central regions of the mean density of the universe at their characteristic formation epoch.

In the two cases analysed (homogeneous and inhomogeneous models), halo concentrations seem to be controlled by both changes in formation epochs of the halo cores as well as by differing virialisation overdensities. While for inhomogeneous models, changes in the virialisation process constitute the most influential factor, for homogeneous models it is the differing formation histories that are most responsible for the changes in concentrations.

Having determined the theoretical $c_{\rm vir} - M_{\rm vir}$ relation, we then deduced the corresponding $\rho_s - r_s$ and $\Delta_{V/2} - V_{\rm max}$ relations which represent physical measures that, unlike the $c_{\rm vir} - M_{\rm vir}$ relation, may establish a more direct link with observations. Here, we note that the homogeneous models manifest more detectable differences in both ρ_s and $\Delta_{V/2}$ than the inhomogeneous models. Specially, the inhomogeneous curves do not register the scaling one might have expected based on the $c_{\rm vir}$ values at fixed mass. This arises because ρ_s and $\Delta_{V/2}$ depend both on $c_{\rm vir}$ and on $\Delta_{\rm vir}(z_o)$ which counterbalance each other. Nonetheless, it is intriguing why inhomogeneous models reveal visible changes in their collapse dynamics and do not show apparent differences in their central densities. This could be associated with the prescription used to calculate the characteristic collapse epoch which may not be applicable to inhomogeneous models. We notice that it is also important to realise that the free parameter $C_\sigma = 28$, whose meaning is in fact unknown, may not be appropriate. Clearly, these assumptions should not be undervalued, and require a test against N–body simulations.

Studying the impact of dark energy on the density structure of dark matter halos surely represents an important step on our understanding of structure formation on those models. Unfortunately, halo properties do not seem to provide a (at present) robust way of probing dark energy. The $\Delta_{V/2} - V_{\rm max}$ and $\rho_s - r_s$ relations are plagued by observational scatter on the data that may (or may not) be associated with selection effects (cooling baryons in the former; hydrostatic equilibrium and isothermal hypothesis in the latter) and by the intrinsic, theoretical in nature, scatter in halo concentration values about the mean which is believed to be due to a spread on the collapse histories of N–body simulated halos. Additionally, there is the implicit uncertainty on the the

value of σ_8 as a function of w which we fixed in this analysis (see discussion in [8]). Nevertheless, the effect of dark energy on the dark matter halo structure may be exploited indirectly through strong and weak lensing statistics. Another alternative path may be the time evolution of dark matter halo abundances [6].

While it is reassuring that the analytical recipe of [17] is successful in reproducing halo concentrations measured in numerical simulations performed in homogeneous dark energy models, more explicitly for SUGRA and Ratra–Peebles potentials [7], it should be recognised that the same recipe has not been tested against simulations carried out in inhomogeneous models. Moreover, one should point out that the methods here used are based on the premise that the halo concentration-mass relation is governed by the ENS model. However, the ENS model is by no means the only viable and popular model. It is just one of a number of theoretical models for how the concentration - mass relation arises. See [18, 19, 44] for other examples of other possibilities. Furthermore, since the Dolag et al. paper [7] (the most recent paper advocating the ENS prescription) there have been a number of developments in studying the halo concentration - mass - redshift relation. Some of these studies produced results in agreement with ENS (e.g. Neto et al. [21]), others find a mass and redshift dependence that contradicts the ENS model (e.g. Maccio et al. [20] and Gao et al. [22]). At present the matter has not been settled, and it is not possible to identify one model that works better than all of the others. A Further investigation using and comparing other prescriptions will appear in a near future work [50].

Ideally, this work will motivate further studies using N–body simulations which, ultimately, will draw a firm conclusion on the interconnection between the dark matter halo structure and the underlying cosmology.

Acknowledgments

We would like to thank C. van de Bruck, A. Lopes, L. Miller and J. Taylor for useful discussions and the referee for useful comments. DFM acknowledges support from the A. Humboldt Foundation and the CNRS Visitor Research Fellowship at the University of Montpellier.

References

[1] Spergel D.N., et al., 2003, ApJ Suppl., 148. 175; J. Dunkley *et al.* [WMAP Collaboration], arXiv:0803.0586 [astro-ph].

[2] Perlmutter S., et al., 1999, ApJ, 517, 565; Riess A.G., et al., 2001, ApJ., 560, 49; Knop R.A., et al., ApJ, 2003, 598, 102.

[3] Carroll S.M., Press W.H. & Turner E.L., 1992, Ann. Rev. Astron. Astrophys., 30, 499; T. Koivisto and D. F. Mota, Astrophys. J. **679** (2008) 1;T. Koivisto and D. F. Mota, JCAP **0806** (2008) 018;A. Balaguera-Antolinez, D. F. Mota and M. Nowakowski, Class. Quant. Grav. **23** (2006) 4497.

[4] Ratra B., Peebles P.,1988, ApJ, 325, L17.

[5] S. M. Carroll, A. De Felice, V. Duvvuri, D. A. Easson, M. Trodden and M. S. Turner, Phys. Rev. D **71** (2005) 063513; T. Koivisto and D. F. Mota, Phys. Rev. D **75** (2007) 023518; T. Koivisto and D. F. Mota, Phys. Lett. B **644** (2007) 104; B. Li, J. D. Barrow and D. F. Mota, Phys. Rev. D **76** (2007) 104047;

[6] Klypin A.A., Macció A.V., Mainini R., Bonometto S.A., ApJ, 2003, 599, 31; P. M. Sutter and P. M. Ricker, arXiv:0804.4172 [astro-ph]; C. Shapiro and S. Dodelson, Phys. Rev. D **76** (2007) 083515.

[7] Dolag K., Bartelmann M., Perrotta F., Baccigalupi C., Moscardini L., Meneghetti M., Tormen G., 2003, preprint astro-ph/0309771.

[8] Kuhlen M., Strigari L.E., Zentner A.R., Bullock J.S. & Primack J.R., 2004, preprint astro-ph/0402210; M. Kuhlen, C. R. Keeton and P. Madau, Astrophys. J. **601**, 104 (2004).

[9] A. Maccio, F. Governato and C. Horellou, Mon. Not. Roy. Astron. Soc. **359** (2005) 941; A. V. Maccio, Mon. Not. Roy. Astron. Soc. **361** (2005) 1250; A. V. Maccio, S. A. Bonometto, R. Mainini and A. Klypin, arXiv:astro-ph/0309439.

[10] L. Gao, V. Springel and S. D. M. White, Mon. Not. Roy. Astron. Soc. Lett. **363**, L66 (2005); E. D'Onghia, C. Firmani and G. Chincarini, Mon. Not. Roy. Astron. Soc. **338** (2003) 156;

[11] Bartelmann M., Meneghetti M., Perrotta F., Baccigalupi C., Moscardini L., 2003, A&A, 409, 449.

[12] Lopes A.M. & Miller L., 2004, MNRAS, 348, 519; P. Schneider, arXiv:astro-ph/0509252; R. L. C. Starling *et al.*, arXiv:astro-ph/0508237; V. Acquaviva and C. Baccigalupi, Phys. Rev. D **74** (2006) 103510; M. Bartelmann, M. Doran and C. Wetterich, arXiv:astro-ph/0507257; H. K. Jassal, J. S. Bagla and T. Padmanabhan, Phys. Rev. D **72** (2005) 103503; B. Li, J. D. Barrow and D. F. Mota, Phys. Rev. D **76**, 044027 (2007); B. Li, D. Fonseca Mota and J. D. Barrow, Phys. Rev. D **77** (2008) 024032; C. Horellou and J. Berge, Mon. Not. Roy. Astron. Soc. **360** (2005) 1393; M. Le Delliou, JCAP **0601** (2006) 021.

[13] C. Fedeli, M. Bartelmann, M. Meneghetti and L. Moscardini, arXiv:0705.3169 [astro-ph].

[14] M. Manera and D. F. Mota, Mon. Not. Roy. Astron. Soc. **371** (2006) 1373; N. J. Nunes and D. F. Mota, Mon. Not. Roy. Astron. Soc. **368** (2006) 751.

[15] Mota D.F. & van de Bruck C., 2004, A&A, 421, 71.

[16] I. Maor and O. Lahav, JCAP **0507** (2005) 003; D. J. Shaw and D. F. Mota, Astrophys. J. Suppl. **174** (2008) 277; R. Mainini, Phys. Rev. D **72** (2005) 083514; W. J. Percival, Astron. Astrophys. **443** (2005) 819; M. Bartelmann, M. Doran and C. Wetterich, arXiv:astro-ph/0507257; P. Wang, Astrophys. J. **640** (2006) 18.

[17] Eke V.R., Navarro J.F. & Steinmetz M., 2001, ApJ, 554, 114.

[18] J. S. Bullock, R. H. Wechsler and R. S. Somerville, Mon. Not. Roy. Astron. Soc. **329**, 246 (2002) [arXiv:astro-ph/0106293]; J. S. Bullock, arXiv:astro-ph/0106380; J. S. Bullock, arXiv:astro-ph/0111005.

[19] A. V. Maccio', A. A. Dutton and F. C. v. Bosch, arXiv:0805.1926 [astro-ph].

[20] A. V. Maccio', I. Sideris, M. Miranda, B. Moore and R. Jesseit, arXiv:0704.3078 [astro-ph].

[21] A. F. Neto *et al.*, arXiv:0706.2919 [astro-ph].

[22] L. Gao *et al.*, arXiv:0711.0746 [astro-ph].

[23] F. Perrotta, S. Matarrese, M. Pietroni and C. Schimd, Phys. Rev. D **69** (2004) 084004;D. F. Mota, J. R. Kristiansen, T. Koivisto and N. E. Groeneboom, Mon. Not. Roy. Astron. Soc. **382** (2007) 793; R. Caimmi, New Astron. **12** (2007) 327; U. Debnath, S. Nath and S. Chakraborty, Mon. Not. Roy. Astron. Soc. **369** (2006) 1961; S. Basilakos and N. Voglis, Mon. Not. Roy. Astron. Soc. **374** (2007) 269; L. R. W. Abramo, R. C. Batista, L. Liberato and R. Rosenfeld, Phys. Rev. D **77** (2008) 067301; C. F. C. Brandt, R. Chan, M. F. A. da Silva and J. F. V. da Rocha, arXiv:0805.2106 [gr-qc]; S. Unnikrishnan, H. K. Jassal and T. R. Seshadri, arXiv:0801.2017 [astro-ph];A. W. Brookfield, C. van de Bruck, D. F. Mota and D. Tocchini-Valentini, Phys. Rev. Lett. **96** (2006) 061301; T. Koivisto and D. F. Mota, Phys. Rev. D **73** (2006) 083502; B. M. Schaefer and K. Koyama, arXiv:0711.3129 [astro-ph]; D. F. Mota, D. J. Shaw and J. Silk, arXiv:0709.2227 [astro-ph]; A. Balaguera-Antolinez, D. F. Mota and M. Nowakowski, Mon. Not.

Roy. Astron. Soc. **382** (2007) 621; D. J. Shaw and D. F. Mota, arXiv:0708.0868 [astro-ph]; K. Kohri, C. M. Lin and D. H. Lyth, JCAP **0712** (2007) 004; L. R. Abramo, R. C. Batista, L. Liberato and R. Rosenfeld, JCAP **0711** (2007) 012; S. Dutta and I. Maor, Phys. Rev. D **75** (2007) 063507; S. Basilakos and N. Voglis, Mon. Not. Roy. Astron. Soc. **374** (2007) 269; R. Caimmi, Serb. Astron. J. **174** (2007) 13; C. P. Burgess, R. Easther, A. Mazumdar, D. F. Mota and T. Multamaki, JHEP **0505** (2005) 067; D. A. Easson, R. Gregory, D. F. Mota, G. Tasinato and I. Zavala, JCAP **0802** (2008) 010; I. Maor, Int. J. Theor. Phys. **46** (2007) 2274; T. Buchert, Class. Quant. Grav. **23** (2006) 817; N. J. Nunes, A. C. da Silva and N. Aghanim, Astron. Astrophys. **450** (2006) 899.

[24] Wetterich C., 2001, Phys. Lett. B, 522, 5; Wetterich C., 2002, Phys. Rev. D, 65, 123512.

[25] L. Amendola, Phys. Rev. D **69** (2004) 103524

[26] Wang L.M. & Steinhardt P.J., 1998, ApJ, 508, 483.

[27] Weinberg N. & Kamionkowski M., 2003, MNRAS, 341, 251; Lahav O., et al., 1991, MNRAS, 251, 128.

[28] Alam S.M.K., Bullock J.S. & Weinberg D.H., 2002, ApJ, 572, 34.

[29] Albrecht A. & Skordis K., 2000, Phys. Rev. Lett., 84, 2076.

[30] Alcubierre A., Guzman F., Matos T., Nunez D., Urena-Lopez L., Wiederhold P., 2002, Class. Quant. Grav., 19, 5017; Guzman F., Urena-Lopez L. 2003, Phys. Rev. D, 68, 024023..

[31] Arbey A., Lesgourgues J., Salati P., 2001, Phys. Rev. D, 64, 123528.

[32] Bardeen J.M., Bond J.R., Kaiser N. & Szalay A.S., 1986, ApJ, 304, 15.

[33] Barreiro T., Copeland E. & Nunes N.J., 2000, Phys. Rev. D, 61, 1273012206.

[34] Bartelmann M., Perrotta F. & Baccigalupi C., 2002, A&A, 396, 21.

[35] Bean R. & Magueijo J., 2002, Phys. Rev. D, 66, 063505.

[36] Brax P. & Martin J. 1999, Phys. Lett. B, 468, 40.

[37] Padmanabhan T., Choudhury T., 2002, Phys. Rev. D, 66, 081301;Padmanabhan T., 2002, Phys. Rev. D 66, 021301; Causse M., 2003, preprint astro-ph/0312206; Bagla J., Jassal H., Padmanabhan T., 2003, Phys. Rev. D, 67, 063504.

[38] Caheng L.-M. & Wu X.-P., 2001, A&A, 372, 281.

[39] L. Liberato and R. Rosenfeld, JCAP **0607** (2006) 009; N. Tetradis, Phys. Lett. B **632** (2006) 463; M. Meneghetti, M. Bartelmann, K. Dolag, L. Moscardini, F. Perrotta, C. Baccigalupi and G. Tormen, New Astron. Rev. **49** (2005) 111;

[40] Ma C.-P., Caldwell R.R., Bode, P. & Wang L., 1999, ApJ, 521, L1.

[41] Macció A.V., Quercellini C., Mainini R., Amendola L., Bonometto S.A., 2003, preprint astro-ph/0309671.

[42] Makino N., Sasaki S. & Suto Y., 1998, ApJ, 497, 555.

[43] Khoury J., Weltman A., 2004, Phys. Rev. D **69** 044026; Khoury J., Weltman A., 2003, preprint astro-ph/0309300; D. F. Mota and D. J. Shaw, Phys. Rev. Lett. **97** (2006) 151102; D. F. Mota and D. J. Shaw, Phys. Rev. D **75** (2007) 063501; Mota D.F., Barrow J.D., 2004a, Phys. Lett. B, 581, 141; Mota D.F., Barrow J.D., 2004b, MNRAS, 349, 281; Clifton T., Mota D.F., Barrow J.D., 2004, preprint gr-qc/0406001.

[44] Navarro J.F., Frenk C.S. & White S.D., 1997, ApJ, 490, 493.

[45] Steinhardt P.J., Wang L. & Zlatev I., 1999, Phys. Rev. D, 59, 123504.

[46] Sugiyama N., 1995, ApJ Supplement Series, 100, 281.

[47] Wechsler R.H., Bullock J.S., Primack J.R., Kravtsov A.V., Dekel A., 2002, ApJ, 568, 52.

[48] Wu X.-P. & Xue Y.-J., 2000, ApJ, 529, L5.

[49] Zentner A.R. & Bullock J.S., 2002, Phys. Rev. D, 66, 043003.

[50] D. F. Mota, work in progress